



AMERICAN METEOROLOGICAL SOCIETY

Monthly Weather Review

EARLY ONLINE RELEASE

This is a preliminary PDF of the author-produced manuscript that has been peer-reviewed and accepted for publication. Since it is being posted so soon after acceptance, it has not yet been copyedited, formatted, or processed by AMS Publications. This preliminary version of the manuscript may be downloaded, distributed, and cited, but please be aware that there will be visual differences and possibly some content differences between this version and the final published version.

The DOI for this manuscript is doi: [10.1175/2010MWR3330.1](https://doi.org/10.1175/2010MWR3330.1)

The final published version of this manuscript will replace the preliminary version at the above DOI once it is available.



**Fine-scale single- and dual-Doppler analysis of tornado intensification,
maintenance, and dissipation in the Orleans, Nebraska, supercell.**

Joshua Wurman, Karen Kosiba,

Center for Severe Weather Research, Boulder, Colorado

Paul Markowski, Yvette Richardson,

The Pennsylvania State University, University Park, Pennsylvania

David Dowell

National Center for Atmospheric Research, Boulder, Colorado

Paul Robinson

Center for Severe Weather Research, Boulder, Colorado

Submitted to Monthly Weather Review

Revised: 11 April 2010

Revised again: 16 August 2010

ABSTRACT

Fine-scale single- and dual-Doppler observations are used to diagnose the three-dimensional structure of the wind field surrounding a tornado that occurred near the town of Orleans, Nebraska, on 22 May 2004. The evolution of the vorticity and divergence fields and other structures near the tornado are documented in the lowest kilometer. Changes in tornado intensity are compared to the position of the tornado relative to primary and secondary gust fronts. Circulation on scales of a few kilometers surrounding the tornado remains relatively constant during the analysis period, which spans the intensifying and mature periods of the tornado's lifecycle. Stretching of vertical vorticity and tilting of horizontal vorticity are diagnosed, but the latter is near or below the threshold of detectability in this analysis during the observation period in the analyzed domain. Low-level circulation within 500 m of the tornado increased several minutes before vortex-relative and ground-relative near-surface winds speeds in the tornado increased, raising the possibility that such trends in circulation may be useful in forecasting tornado intensification.

1. Introduction

Although tornadic storms have been observed by radar for decades (e.g., Stout and Huff 1953; Ludlam 1963; Fujita 1975; Ray 1975, 1981; Brandes 1977, 1978, 1981, 1984; Klemp et al. 1981; Dowell and Bluestein 1997, 2002a,b; Wakimoto and Liu 1998; Trapp 1999; Wakimoto and Cai 2000; Bluestein and Gaddy 2001), the resolution often was too coarse to resolve accurately the structural details on spatial scales less than 1 km. However, with the advent of mobile radars (Bluestein et al. 1993, 1995; Wurman et al. 1997; Bluestein and Pazmany 2000; Wurman and Randall 2001; Wurman et al. 2008), single-Doppler (Wurman et al. 1996ab; Wurman and Gill 2000; Wurman 2002; Bluestein et al. 1996, 2000, 2003, 2004; Alexander and Wurman 2005; Wurman and Alexander 2005; Lee and Wurman 2005; Dowell et al. 2005; Tanamachi et al. 2007; French et al. 2008, Kosiba and Wurman 2010) and, occasionally, dual-Doppler (Richardson et al. 2001; Dowell et al. 2002; Beck et al. 2006; Wurman et al. 2007a,b; Marquis et al. 2008; Frame et al. 2009) data sets that resolve sub-kilometer scale features in supercell thunderstorms have become available. These latter fine-scale data have permitted the dual-Doppler synthesis of vector wind fields at spatial and temporal intervals of $\Delta x \sim O[100 \text{ m}]$ and $\Delta t \sim O[10\text{-}100 \text{ s}]$, respectively, thereby allowing derivation of dynamically important quantities such as divergence, vorticity, and the stretching and tilting of vorticity, on the sub-kilometer scale and rapidly evolving features present near tornadoes.

Wurman et al. (2007a) presented a two-dimensional analysis of tornadogenesis and the subsequent tornado associated with a storm merger near Kiefer, Oklahoma, and hypothesized that the merger caused both the genesis and the later demise of the second,

weaker tornado. Additionally, the existence of a secondary rear-flank gust front was documented. [Whether these features were actual secondary gust fronts, with density differences across the fronts, was not confirmable with observations. In some tornadic storms, these secondary structures may not be associated with density discontinuities and would be more accurately described as “secondary convergence lines” which form behind the rear flank gust front and therefore do not separate inflow and outflow air masses (J. Marquis 2009, personal communication). In this paper, we follow the terminology of Wurman et al. (2007a) and Marquis et al. (2008).] Wurman et al. (2007b) conducted an analysis of the three-dimensional wind field of a tornado near Bridgeport, Nebraska, diagnosing terms in the vorticity budget associated with the maintenance of the tornado. No double gust front was observed. Parcels at a few hundred m AGL in the immediate vicinity of the tornado were calculated to have experienced both tilting and stretching of vorticity, as revealed in a dual-Doppler analysis for a single observation time. However the magnitude of the tilting and stretching experienced by air parcels was not calculated through trajectory analysis.

Using well-synchronized dual-Doppler data, Dowell et al. (2002) calculated air parcel trajectories for a tornado near Argonia, Kansas. The trajectory analysis revealed that, at 250 m, air parcels entered the tornado from behind the gust front to the north of the mesocyclone and from ahead of the gust front to the southeast of the mesocyclone, indicating two source regions for the air that entered the tornado. The updraft structure also showed rapid evolution from a linear structure to a comma shape during the period of mesocyclogenesis, while the rear flank downdraft became more coherent. However,

given that this was a relatively weak and short-lived tornado, it is not clear whether these results are transferable to more significant or longer-lived tornadoes.

Using similar dual-Doppler and trajectory analysis techniques, Marquis et al. (2008) diagnosed the low-level evolution of a tornado and its surrounding flow near Crowell, Texas, on 30 April 2000. A secondary gust front was observed behind the primary rear flank gust front leading to a double gust front structure. Trajectory analysis revealed the ascent of rear-flank downdraft air parcels along the secondary gust front. Further, the secondary gust front, which came into very close proximity, wrapping around the tornado, was observed to affect the convergence field surrounding the tornado. During this period of interaction, the tornado structure and intensity underwent significant evolution, developing an asymmetric vertical vorticity structure with multiple vertical vorticity maxima along the western flank of the vorticity pattern.

To date, only three tornadic storms, Kiefer, Bridgeport, and Crowell, have been presented in the formal literature using dual-Doppler vector wind field retrievals at very fine scale resolution from mobile ground-based radars. Additional studies are needed to assess the generalness of the results and hypotheses presented in these works, including the prevalence of secondary gust fronts, and how these relate to tornado evolution. This paper presents the analyses of one of the rare fine-scale dual-Doppler data sets collected in a tornadic supercell near Orleans, Nebraska, on 22 May 2004. Some aspects of the dual-Doppler data set are not ideal, particularly the starting time (after tornadogenesis), the duration (only 11 minutes), and the depth (only up to 1 km AGL). In addition, the

scanning of the two DOWs was not well synchronized. Finally, there was a gap in data collection by one DOW while it repositioned. Nevertheless, the quality of available data during the intensifying and mature stages of a tornado make this case important for documentation and thus for comparison to previous and future cases. The evolution of the three-dimensional winds revealed processes that may underlie the maintenance and eventual demise of the Orleans tornado. Contributions to the vertical vorticity tendency and distribution were diagnosed from dual-Doppler observations. Features observed in this storm were compared to those observed in prior dual-Doppler studies.

2. Storm-scale evolution of the Orleans, Nebraska, tornadic supercell

The environment on 22 May 2004 was favorable for the development of organized convection across the central plains of the United States. The 0000 UTC Storm Prediction Center Severe Weather Composite Map (not shown) depicted CAPE values of approximately 2500 J kg^{-1} in a moderately capped environment with CIN of 100 J kg^{-1} . However, the analysis is coarse and may not have been precisely representative of conditions near the tornadic storm crossing near Orleans, Nebraska. The high instability in conjunction with 0-6 km shear of approximately $33 \text{ m s}^{-1} / 6 \text{ km}$ and an estimated 0-3 km storm-relative helicity of $225 \text{ m}^2 \text{ s}^{-2}$, was conducive to severe convection (Weisman and Klemp 1984; Davies-Jones et al. 1990; Brooks et al. 2003).

The National Weather Service WSR-88D located in Hastings, Nebraska (KUEX), observed the storm that produced a tornado near Orleans, Nebraska. A supercell

thunderstorm with reflectivity approaching 65 dBZ along with other smaller storms moved generally eastward from 2100 UTC until after 0000 UTC (all times hereafter are UTC), when the convection grew upscale. By 2207:52, a prominent hook echo was evident in the lowest elevation scan [the 0.5° scan was about 2 km AGL at a range of 145 km (Doviak and Zrnich 1984)], and a bounded weak echo region was identified above the 0.5° scan (not shown). During the later Doppler on Wheels (DOW) dual-Doppler period, the storm was at a range of approximately 100 km from the KUEX; thus, the lowest level scans were about 1 km AGL, and azimuthal sampling interval at this range was approximately 1.6 km. A hook echo and mesocyclone were evident in the WSR-88D data throughout the dual-Doppler synthesis period, from 2259 through 2310 (Figure 1). As will be discussed below, this mesocyclone was associated with a tornado observed by the DOW mobile radars from 2253 through 2312. By 2310, the protuberance at the southwestern corner of the storm no longer exhibited a hook shape and there was only very weak circulation remaining in the low-level mesocyclone signature evident in the WSR-88D data. The peak gate-to-gate azimuthal velocity differential across the mesocyclone from the WSR-88D Level-3 data was observed at 2255 and was 13.4 m s^{-1} (26 knots) across the mesocyclone. A small area of precipitation, initially located to the southeast of the hook echo at 2255, moved northward and impinged on the hook of the primary storm after 2305, when the tornado (see below) was already dissipating.

3. Doppler On Wheels deployment and dual-Doppler synthesis

a. Description of the radars

The 3-cm wavelength DOW mobile radars (Wurman et al. 1997, 2008; Wurman 2001) were developed for the express purpose of obtaining high-resolution data in tornadoes and other small-scale and short-lived phenomena. In this study, the 2004-vintage DOWs used 500 ns gate lengths and pulses to achieve range resolution of 75 m out to a range of 24 km to optimize dual-Doppler syntheses. Parabolic antennas with a 2.44 m diameter produced half-power beam widths of 0.93° . The DOWs oversampled in azimuth to achieve sample spacing of approximately 100 m. The DOWs operated at 9.37 GHz, with a peak transmit power of 250 kW, making them capable of retrieving data in the clear-air boundary layer surrounding tornadic storms. As the transmitted power, system losses and receiver noise levels and gain were not well characterized, radar reflectivity levels were uncalibrated.

b. Deployment and single-Doppler observations of storm structure

The DOW2 and DOW3 radars deployed along US Highway 183 to the east and northeast of Orleans, Nebraska (Figure 2). The DOW baseline was 7.1 km and was to the east of the approaching hook of the supercell (Figure 1). The DOW3 radar was deployed and level to within 0.2° at 2253:48, and the DOW2 radar was deployed and level to within 0.2° at 2257:58. The leveling tolerance was much less than the half power beamwidth, so

resultant errors in vertical navigation of less than 40 m would be insignificant to the dual-Doppler analysis, which was conducted on a grid with 100 m spacing. Volumetric single Doppler data, extending from about 100 m AGL to 1.2 km AGL at the range of the tornado, were collected from 2253 to 2258 (Figure 3).

Raw single-Doppler fields, which have not been objectively analyzed onto Cartesian grids, reveal the evolution of some structures associated with the tornado and provide confidence in the objectively analyzed fields and dual-Doppler-retrieved quantities (discussed in Section 3). The reflectivity observations of the storm revealed a coiled hook with a low-reflectivity eye in the lowest elevations, which became more diffuse with height, similar in appearance to many DOW observations of non-multiple vortex tornadoes (e.g. Wurman et al. 1996, Dowell et al. 2005). Correspondingly, in the Doppler velocity field, the low-reflectivity eye is coincident with a circulation with a diameter of 900 m (as defined by the distance between outbound and inbound velocity extrema) and a velocity differential (ΔV ; the difference between the inbound and outbound Doppler velocity extrema) of 51 m s^{-1} at the lowest observation level of 100 m AGL. At the initial single Doppler observation time, a weak tornado was evident in the radar data and a condensation funnel was visible (Figure 4). The primary rear-flank gust front (PRFGF) was associated with a line of convergence to the north and east of the tornado. The PRFGF sloped inward with height toward the tornadic circulation; at 65 m AGL the PRFGF was located approximately 6 km from the tornado (Fig. 3: 0.3° panels), whereas at 985 m AGL the PRFGF was only 3.3 km from the tornado (Fig. 3: 4.0° panels). Behind the hook, to the west-southwest of the tornado, a region of radial

velocity divergence suggestive of horizontal divergence at the lowest observed levels demarked the rear-flank downdraft (RFD). The radial divergence associated with the RFD is only observed in the lowest elevation scans, below ~ 400 m, and could thus only be resolved well with very proximate radar observations.

As the dual-Doppler observation period commenced at 2259 (after the tornado had formed), observations from the individual DOW radars revealed that the hook had become enfolded into the storm (Figure 5). Previous observations of tornadic storms have identified this morphology in weak (Wurman et al. 2007a) and/or dissipating (Wurman and Gill 2000; Alexander and Wurman 2005) tornadoes, in contrast to “healthier” tornadoes that maintained a distinct separate hook feature. Although simultaneous in situ data have not been available to provide supporting evidence, one plausible hypothesis is that these former tornadoes weakened owing to the ingestion of negatively buoyant, rain-cooled outflow air. As the hook was increasingly enfolded with time, it merged with the parent storm. At 2304, the clear reflectivity eye was barely discernible, and by 2307 it was no longer present. The velocity data from during this period reveal that the tornado exhibited its highest wind speeds at 2307 and then quickly weakened thereafter. Throughout this period, the PRFGF was well ahead of the tornado, suggesting a separation of the updraft associated with the tornadic circulation from what is likely to be more buoyant inflow air in the main updraft at low levels, as has been observed in early dual-Doppler analyses (e.g., Brandes 1977). Importantly, beginning at 2307, there was evidence of a region of weak cyclonic convergence to the north of the tornadic circulation in the DOW2 velocity field (denoted by an “X” in Fig. 5). This

region of convergence may be indicative of the primary updraft being located well north of the tornado, over the new circulation that formed to the north of the tornado. The development of this circulation occurred simultaneously with the tornado's demise. This new circulation did not develop into a subsequent tornado detectable by the DOWs or nearby visual observation.

Discernible in the early single-Doppler (DOW2) velocity observations (but more clearly obvious in dual-Doppler analysis, discussed below) was the presence of a secondary rear-flank gust front (SRFGF) that was located behind the PRFGF in a region of precipitation south of the tornado (Figure 5). It was manifested as a line of weak radial convergence, implying probable horizontal convergence, to the south of the tornado. The primary and secondary gust fronts were unconnected, which is in contrast to the DOW observations of gust fronts in the Kiefer, Oklahoma, tornadic storm (Wurman et al. 2007a), but comparable to the DOW observations of the Crowell, Texas, tornadic storm (Marquis et al. 2008). The possible ramifications of this configuration will be discussed later in the context of the dual-Doppler analysis.

The DOWs were able to observe the core flow region of the tornado from a range starting at approximately 14 km and ending at approximately 7 km (albeit with likely degraded maximum resolved velocities at the larger ranges since the DOW beam width was an appreciable fraction of the core flow diameter, e.g., Brown and Wood 1991). At low levels a reflectivity ring with morphology highly suggestive of a debris and/or precipitation ring was evident (Wurman et. al 1996b, Wurman and Gill 2000, Dowell et

al. 2005, Bluestein et al. 2007), and the core flow radius, maximum winds, and precise position of the center were discernible (Figure 6). These observations facilitated the detailed tracking of the tornado along with the objective characterization of axisymmetric vertical vorticity, radius of maximum winds, and peak ground-relative winds, as well as the translational speed, which is required for dual-Doppler retrievals (Figure 7). As mentioned above, the initial observations obtained by the DOW3 radar revealed that the storm was already producing a weak and broad tornado by 2253. The initial single-Doppler observation of the tornado indicated a peak velocity of 35 m s^{-1} below 100 m AGL and a core flow diameter (Δx) of approximately 900 m. Correspondingly, the peak vertical vorticity, estimated as twice the difference between the maximum outbound and inbound Doppler velocities divided by the distance between the maximum inbound and outbound Doppler velocities, $2\Delta V/\Delta x$, was 0.11 s^{-1} , which was similar in magnitude to other weak tornadoes for which the core flow region has been reasonably well resolved (Dowell et al. 2002; Bluestein et al. 2003; Wurman et al. 2007abc), but substantially lower than the vorticity observed in other, stronger, tornadoes (Wurman et al. 1996; Wurman and Gill 2000; Bluestein et al. 2003; Alexander and Wurman 2004; Alexander and Wurman 2005; Lee and Wurman 2005). After 2255:50, the low-level circulation of the tornado itself (estimated at the radius of maximum winds of the tornado from the 0.6° DOW scans using $\pi*\Delta V*\Delta x$) decreased from over $10^5 \text{ m}^2 \text{ s}^{-1}$ to $3 \times 10^4 \text{ m}^2 \text{ s}^{-1}$ by 2300. This decrease was coincident with the decreased size of the vortex. Consequently, the increase in peak tornado vorticity immediately after 2255, from 0.1 s^{-1} to 0.7 s^{-1} during this same period was likely a result of the contraction of the tornado vortex. There was a rapid increase in tornado ΔV after 2300:57, from about 60 m s^{-1} to a peak of 108 m s^{-1} at

2306:54. During this time the spatial scale of the tornado remained nearly constant with a core flow diameter near 200 m. The circulation doubled from $3 \times 10^4 \text{ m}^2 \text{ s}^{-1}$ to about $6\text{-}8 \times 10^4 \text{ m}^2 \text{ s}^{-1}$, indicating generation and/or transport of angular momentum inward to the radius of maximum winds; however the relative roles of these two processes were not determined. The radar-derived vertical vorticity increased to over 1.0 s^{-1} by 2306. After 2306:54, ΔV and circulation steadily decreased until 2312:12 when the remnant circulation is sub-tornadic according to the criteria set forth in Alexander and Wurman (2008). The implied vertical vorticity decreased to 0.4 s^{-1} as the tornado weakened.

c. Dual-Doppler analysis

At the beginning of the dual-Doppler analysis period (2259), the tornado was approximately 14 km from each DOW, with a 30° inter-beam crossing angle. DOW2 and DOW3 conducted volume scans through 170° and 107° sectors, respectively, at elevation angles of 1.0° , 1.5° , 2.0° , 2.5° , 3.0° , 4.0° , 5.0° , 6.0° , 7.0° , and 9.0° , which provided coverage from approximately 100 m to 2.0 km AGL. Some volumes had data below 1.0° and/or above 9.0° and these were used in the dual-Doppler synthesis. Ideally, the two radars would scan a particular point in space at exactly the same time, so that the radial velocity measurements being combined differ only owing to the differing viewing angles of the radars and not owing to the temporal evolution of the storm between the two data collection times. However, for this case, scanning was not perfectly synchronized, and resulting errors were mitigated by allowing only data that were contemporaneous to within 30 s to be used to create the dual-Doppler syntheses. Dual-Doppler volumes were

created at the following seven times: 2259, 2300, 2301, 2303, 2307, 2309, and 2310. No low elevation sweeps were available from DOW3 from 2304-2306, owing to the reorientation of that radar, so no dual-Doppler synthesis was attempted for that period.

In order to facilitate dual-Doppler analysis, the radar data were interpolated to a common Cartesian grid using a 2-pass Barnes filter. A second-pass convergence parameter (γ) of 0.3 was chosen based on the experiments of Majcen et al. (2008). The grid parameters used in the objective analysis were based on the coarsest azimuthal data spacing (δ) within the dual-Doppler analysis region. For a 0.93° half-power beam width (θ) at a range (R) of 14 km, this results in $\delta = 0.227$ km. Consistent with the radar data spacing, a smoothing parameter [$\kappa = (1.33\delta)^2$] of 0.095 km^2 (Pauley and Wu 1990) and a grid spacing ($\Delta = \delta/2.5$) of 100 m were chosen (Koch et al. 1983). In order to correct for storm motion, an advection correction was applied to each dual-Doppler volume, adjusting the data to a common time. Vertical velocities were derived from upward integration of the continuity equation with a lower boundary condition of $w = 0$ and linear extrapolation of the low-level convergence. The dual-Doppler grid comprised a $20 \text{ km} \times 20 \text{ km}$ area in the horizontal and 1 km in the vertical. Whereas the grid spacing did not properly resolve the tornado core flow (recall that the core flow diameter is close to 200 m during the entire dual-Doppler analysis period), it did resolve many of the larger-scale features associated with the tornadic storm (e.g., the rear-flank downdraft, multiple gust fronts, etc.) that were likely critical to tornado evolution and sustenance.

The dual-Doppler analysis of the rear flank of the storm revealed several features also found within conceptual models (e.g., Lemon and Doswell 1979), modeling studies (e.g., Wicker and Wilhelmson 1995; Adlerman 2003) and other dual-Doppler observations (Richardson et al. 2001; Dowell et al. 2002; Wurman et al. 2007a; Wurman et al. 2007b; Marquis et al. 2008). Similar to the Kiefer, Oklahoma (Wurman et al. 2007a), Bridgeport, Nebraska (Wurman et al. 2007b) and Crowell, Texas (Marquis et al. 2008) tornadoes, the Orleans, Nebraska, tornado was located within a gradient of vertical motion when near its peak intensity from 2306-2309 (Figure 8 and Figure 9def), but with net positive vertical velocity over the tornado at most times (Figure 8 and Figure 9 all panels). The analysis also shows the wrapping of the RFD around the tornadic circulation, as indicated by both the divergent flow to the west-southwest of the tornado, and the location of the PRFGF, the zone of strong convergence to the east and north of the tornado (Figures 8 and 9). Further, the presence of a SRFGF, as documented by Wurman et al. (2007b) and Marquis et al. (2008), persisted through the dual-Doppler analysis period. These features are coherent through the depth of the analysis domain (Figures 8).

At all analysis times, as depicted in the low-level (100 m) horizontal and vertical velocities, the PRFGF is well to the north and east of the tornadic circulation (Figure 9). Although there is strong upward motion along the PRFGF, consistent with the ascent of environmental air over the denser outflow air, there is a large separation between the location of inflow air ascent and the tornadic circulation. While we have no direct evidence that the outflow air is denser, this is suggested by the slope of the PRFGF.

Gradually in time, throughout the depth of the analysis domain to the north of the tornado, a large bulge in the PRFGF developed and slowly increased in separation from the tornadic circulation. Correspondingly, the peak tornadic winds and vertical vorticity quickly decreased in magnitude after 2307. Trajectory analysis, which could have confirmed this possibility, would not be very enlightening owing to the short duration of dual-Doppler observations, just eleven minutes, with two missing volumes, and the shallow depth of the analysis domain, which extended to just 1 km AGL.

The SRFGF was initially located to the south and west of the tornado (Figure 9) and just ahead of a localized downdraft (labeled 'D' in Fig. 9a and 9b), suggestive of its origin. This is similar to the Crowell, Texas tornadic storm analyzed by Marquis et al. (2008), who noted the SRFGF was adjacent to a region of low-level divergence. Marquis et al. (2008) hypothesized that the SRFGF in the Crowell, Texas tornadic storm was associated with either an occlusion downdraft or a heat burst. But, without diagnosing causality of the downdraft a definitive conclusion cannot be drawn using the data analyzed in this study. East of the SRFGF interface, there was little tornado-relative flow, and there was slow ascent along the interface as the interface move eastward. Similar to the findings of Marquis et al. (2008) for the Crowell, Texas, storm, but contrary to the findings of Wurman et al. (2007a) for the Kiefer, Oklahoma, storm, the SRFGF was initially observed to connect with the convergence field immediately surrounding the tornado and did not intersect the PRFGF (Figure 9).

The SRFGF persisted throughout the dual-Doppler analysis period and began to surge forward at 2307 as the rear-flank downdraft increased in horizontal coverage and wrapped into the tornadic circulation. By 2309, the downdraft encircled the tornado to the east and northeast. Although the start of this forward surge was coincident with the maximum observed wind speeds, the tornado quickly diminished in intensity thereafter. The development of the new circulation to the northeast of the tornado along the PRFGF and the surge of the SRFGF away from the tornado were concurrent with tornado demise. The closest tangent point of the SRFGF from 2300-2305 was 1.4-2.2 km, during which time the tornado intensity increased or was approximately steady (Figure 10). After the SRFGF surged away from the tornado, to a distance of 2.4 km by 2309, the tornado rapidly weakened. It is not clear whether the increase in separation from 1.4-2.4 km was related directly to tornado demise.

The rapid decrease in peak winds after 2307 (see Figure 3) was contemporaneous with the weakening of both convergence and variations in vertical velocity in the region surrounding the tornado, and a weakened mechanism for stretching, so that it was likely any additional generation or transport of vorticity was no longer able to overcome the dissipating effects of turbulent mixing.

An attempt was made to map regions experiencing tilting of horizontal vorticity at several analysis times. However, the signal is weak and in some areas is dominated by short-wavelength features that are likely analysis artifacts. However, it should be noted that these calculations were of instantaneous values, not integrated along trajectories. If a

longer and deeper dual-Doppler data set was available, we speculate that any tilting effects contributing to the development of low-level vorticity could have been diagnosed through integration along trajectories.

In the Orleans, Nebraska storm, vertical vorticity values analyzed from the dual-Doppler observations of the tornado approached 0.40 s^{-1} , less than the values derived from the raw Doppler velocities, which reached over 1.0 s^{-1} after 2306, but consistent with the smoothing of the interpolation scheme and the inability of the dual-Doppler analysis to resolve the inner-core region of the tornado. At 2307, at the lowest level ($z = 100 \text{ m}$), a region of enhanced cyclonic vertical vorticity to the south-southwest through southeast and east of the tornado was associated with the divergent flow of the downdraft. The maximum vertical vorticity outside the tornado at a height of 600 m, though, was located along the PRFGF (Figure 11). The low-level and mid-level vertical vorticity distributions prior to the time of maximum tornadic intensity (2307) were qualitatively similar to the vorticity distribution at 2307 (Figure 11c). The vertical vorticity values were slightly larger than when the tornado reached its maximum wind speeds. Neither the peak wind speed nor the peak vertical vorticity values can, by themselves, well describe the intensity of a tornado vortex.

d. Discussion

An important question relating to tornadogenesis and tornado maintenance is how the evolution of the low-level angular momentum surrounding the tornado gets converted

into the vertical vorticity associated with the tornado. In order to explore the evolution of the total angular momentum surrounding this tornadic circulation, the total circulation of the flow surrounding the tornado was calculated from the vector wind fields at a height of 100 m (Figure 12). Generally, the circulation increased with increasing radius, with the largest increases occurring immediately away from the tornado center. At all radii, there was very little change in circulation as a function of time. This finding is similar to Wurman et al. (2007a), who found the magnitude of circulation at a radius of 1.4 km from a tornado center to be relatively constant in time. Whereas the peak winds in the Kiefer tornado (Wurman et al. 2007a) weakened with time, the peak winds and vorticity in the Orleans tornado increased substantially then decreased during the analysis period. The values of circulation in the current study, calculated at a radius of 1.4 km, ranged from $0.8 \times 10^5 \text{ m}^2\text{s}^{-1}$ to $0.9 \times 10^5 \text{ m}^2\text{s}^{-1}$, which were smaller than the circulation values of $1.2 \times 10^5 \text{ m}^2\text{s}^{-1}$ observed in the Kiefer tornado (Wurman et al. 2007a) and less than half of the $4.0 \times 10^5 \text{ m}^2\text{s}^{-1}$ documented in the Bridgeport tornado (Wurman et al. 2007b). Given that the resolutions of the analyses were similar; these difference in magnitude were not likely an analysis artifact, particularly the differences between the Orleans and Bridgeport circulations.

At the lowest analysis level (100 m AGL), a dipole of stretching and compression of vertical vorticity ($\zeta \frac{\partial w}{\partial z}$), similar in appearance to that immediately adjacent to the Bridgeport, Nebraska, tornado, as depicted in Wurman et al. (2007b), was only present in the Orleans, Nebraska, tornado in the 2300 analysis field (Figure 13). This stretching/compression dipole was associated with convergence/divergence proximal to

the tornado. During intensification, depicted at 2303, an annulus of stretching surrounds a region of compression. A similar pattern was observed in the Crowell, Texas tornado (Marquis et al. 2008), where the stretching of vertical vorticity was proximal to strong convergence/upward motion and the compression is associated with impinging downward motion. Although the calculated stretching field is noisy, these structures are both persistent in time and consistent with the previous studies, as noted. But, by 2307, the stretching of vertical vorticity diminished in intensity as the convergence/updraft near the tornado also had decreased in strength. Away from the tornadic circulation, stretching of vertical vorticity occurred in conjunction with the convergence associated with the PRFGF. A broad but weak stretching/compression dipole signal develops in the northern circulation by 2307.

The current analysis did not reveal any coherent regions of tilting of horizontal vorticity in the lowest analysis level (100 m AGL). Given the limitations of the available data coupled with the retrieval accuracy, it is possible that either the instantaneous tilting of horizontal vorticity was not resolved and/or that no significant tilting occurred during the observation period. Appreciable tilting may have occurred well before the observation period, perhaps even before tornadogenesis. In this case, the increase in tornado intensity, as diagnosed by peak ground-relative velocities and $\Delta-V$'s, was caused by the stretching of vertical vorticity already available at low levels within 1.4 km of the center of the tornado.

4. Conclusions

Although the 22 May 2004 Orleans, Nebraska tornado was neither strong nor long-lived, high-resolution dual-Doppler data collected from the DOW radars allowed for analysis of several features and processes critical to tornado sustenance. The evolution of the PRFGF and SRFGF suggested that the storm was not dynamically conducive to producing and/or maintaining a vigorous tornado. The PRFGF was located well ahead of the tornado at all heights throughout the observation period. Additionally, a new circulation developed to the northeast of the tornado, suggesting that the parent storm updraft had moved well north of the existing tornado. Owing to this separation and deflection of the inflow, it was likely that the absence of potentially buoyant air ingestion dampened the stretching of vertical vorticity. As in other weak tornadoes, the vorticity analysis did not reveal any significant vertical vorticity away from the tornado, which is consistent with the slow increase in circulation with increasing radius from 1000 m to 3500 m (Figure 12). Although near-surface velocities are not resolved in the current analysis, very little tilting of horizontal vorticity at all analysis levels (100m – 1000m) was diagnosed near the primary tornadic circulation. Either very weak tilting was present but not observable, or more substantial tilting ceased before the analysis period and stretching of the existing vertical vorticity was the mechanism through which the tornado intensified and was maintained. It also is possible substantial tilting occurred above the 1 km domain.

Circulation surrounding the tornado remained relatively constant throughout the analysis period suggesting that inward radial advection of circulation was offset by the dissipation of angular momentum. It is important to note that the maximum in low-level angular momentum preceded the maximum $\Delta-V$ by at least eight minutes. This has implications for the forecasting of tornado intensification. Specifically there may be an identifiable lead-up signature to tornado intensification. This assertion needs to be evaluated in the context of stronger, longer-lived tornadoes. Additionally, observing this peak in the low-level angular momentum would require moderately fine-scale radar observations (e.g. CASA; Potvin et al. 2009) capable of estimating, even if only approximately, the peak winds and diameter of ongoing tornadoes.

References

- Adlerman, E. J., 2003: Numerical simulations of cyclic storm behavior: Mesocyclogenesis and tornadogenesis. Ph.D. dissertation, University of Oklahoma, 217 pp. [Available from School of Meteorology, University of Oklahoma, 100 East Boyd, Suite 1310, Norman, OK 73019.]
- Alexander, C. R., and J. Wurman, 2005: The 30 May 1998 Spencer, South Dakota, storm. Part I: The evolution and environment of the tornadoes. *Mon. Wea. Rev.*, **133**, 72–96.
- Alexander, C. R., and J. Wurman, 2008: Updated mobile radar climatology of supercell tornado structures and dynamics. Preprints, *24th Conf. on Severe Local Storms*, Savannah, GA, Amer. Meteor. Soc.
- Barnes, S. L., 1964: A technique for maximizing details in numerical weather map analysis. *J. Appl. Meteor.*, **3**, 396–409.
- Beck, J.R., J. Schroeder, and J. Wurman, 2006: High-resolution dual-Doppler analyses of the 29 May 2001 Kress, Texas, cyclic supercell. *Mon. Weather Rev.*, **134**, 3125–3148.
- Bluestein, H. B., and W. P. Unruh, 1993: On the use of a portable FM-CW Doppler radar for tornado research. *The Tornado: Its Structure, Dynamics, Predication, and Hazards, Geophys. Monogr.*, No. 79, Amer. Geophys. Union, 367–376.
- , A. L. Pazmany, J. C. Galloway, and R. E. Mcintosh, 1995: Studies of the substructure of severe convective storms using a mobile 3-mm-wavelength Doppler radar. *Bull. Amer. Meteor. Soc.*, **76**, 2155–2170.
- , and ———, 2000: Observations of tornadoes and other convective phenomena with a mobile, 3-mm wavelength, Doppler radar: The spring 1999 field experiment. *Bull. Amer. Meteor. Soc.*, **81**, 2939–2951.
- , and S. G. Gaddy, 2001: Airborne pseudo Dual-Doppler analysis of a rear-inflow jet and deep convergence zone within a supercell. *Mon. Wea. Rev.*, **129**, 2270–2289.
- , C. C. Weiss, and A. L. Pazmany, 2003: Mobile Doppler radar observations of a tornado in a supercell near Bassett, Nebraska, on 5 June 1999. Part I: Tornadogenesis. *Mon. Wea. Rev.*, **131**, 2954–2967.
- , ———, and ———, 2004: The vertical structure of a tornado: High-resolution, W band, Doppler radar observations near Happy, Texas, on 5 May 2002. *Mon. Wea. Rev.*, **132**, 2325–2337.

- , M. M. French, R. L. Tanamachi, S. Frasier, K. Hardwick, F. Junyent, and A. L. Pazmany, 2007: Close-range observations of tornadoes in supercells made with a dual-polarization, X-band, mobile Doppler radar. *Mon. Wea. Rev.*, **135**, 1522–1543.
- Brandes, E. A., 1977: Gust front evolution and tornado genesis as viewed by Doppler radar. *J. Appl. Meteor.*, **16**, 333–338.
- , 1978: Mesocyclone evolution and tornadogenesis: Some observations. *Mon. Wea. Rev.*, **106**, 995–1011.
- , 1981: Fine structure of the Del City–Edmond tornadic mesocirculation. *Mon. Wea. Rev.*, **109**, 635–647.
- , 1984: Vertical vorticity generation and mesocyclone sustenance in tornadic thunderstorms: The observational evidence. *Mon. Wea. Rev.*, **112**, 2253–2269.
- Brooks, H. B., J. W. Lee, and J. P. Craven, 2003: The spatial distribution of severe thunderstorm environments from global reanalysis data. *Atmos. Research*, **67–68**, 73–94.
- Brown, R. A. and V. T. Wood, 1991: On the interpretation of single Doppler velocity pattern within severe thunderstorms. *Wea. Forecasting*, **6**, 32–48.
- Carbone, R. E., M. J. Carpenter, and C. D. Burghart, 1985: Doppler radar sampling limitations in convective storms. *J. Atmos. Oceanic Technol.*, **2**, 357–361.
- Davies-Jones, R. P., D. Burgess, and M. Foster, 1990: Test of helicity as a tornado forecast parameter. Preprints, *16th Conf. on Severe Local Storms, Kananaskis Park, AB, Canada*, Amer. Meteor. Soc., 588–592.
- Dowell, D. C., and H. B. Bluestein, 1997: The Arcadia, Oklahoma, storm of 17 May 1981: Analysis of a supercell during tornadogenesis. *Mon. Wea. Rev.*, **125**, 2562–2582.
- , and ———, 2002a: The 8 June 1995 McLean, Texas, storm. Part I: Observations of cyclic tornadogenesis. *Mon. Wea. Rev.*, **130**, 2626–2648.
- , and ———, 2002b: The 8 June 1995 McLean, Texas, storm. Part II: Cyclic tornado formation, maintenance, and dissipation. *Mon. Wea. Rev.*, **130**, 2649–2670.
- , Y. Richardson, and J. Wurman, 2002: Observations of the formation of low-level rotation: The 5 June 2001 Sumner County, Kansas, tornado. Preprints, *21st Conf. on Severe Local Storms, San Antonio, TX*, Amer. Meteor. Soc., 12.3. [Available online at <http://ams.confex.com/ams/pdfpapers/47335.pdf>.]

- , C. R. Alexander, J. M. Wurman, and L. J. Wicker, 2005: Centrifuging of hydrometeors and debris in tornadoes: Radar-reflectivity patterns and wind measurement errors. *Mon. Wea. Rev.*, **133**, 1501–1524.
- Frame, J., P. Markowski, Y. Richardson, J. Straka, and J. Wurman, 2009: Polarimetric and dual-Doppler radar observations of the Lipscomb County, Texas, supercell thunderstorm on 23 May 2002. *Mon. Wea. Rev.*, **137**, 544–561.
- French, M.M., H.B. Bluestein, D.C. Dowell, L.J. Wicker, M.R. Kramar, A.L. Pazmany, 2008: High-resolution, mobile Doppler radar observations of cyclic mesocyclogenesis in a supercell. *Mon. Wea. Rev.* **136**, 4997–5016.
- Fujita, T. T., 1975: New evidence from the April 3-4, 1974 tornadoes. Preprints, *Ninth Conf. on Severe Local Storms*, Norman, Oklahoma, Amer. Meteor. Soc., 248–255.
- , and R. M. Wakimoto, 1982: Anticyclonic tornadoes in 1980 and 1981. Preprints, *12th Conference on Severe Local Storms*, San Antonio, Texas, Amer. Meteor. Soc., 401–404.
- Jenson, B., T. P. Marshall, M. A. Mabey, and E. N. Rasmussen, 1983: Storm scale structure of the Pampa storm. Preprints, *13th Conference on Severe Local Storms*, Tulsa, OK, Amer. Meteor. Soc., 85–88.
- Klemp, J. B., R. B. Wilhelmson, and P. S. Ray, 1981: Observed and numerically simulated structure of a mature supercell thunderstorm. *J. Atmos. Sci.*, **38**, 1558–1580.
- , and R. Rotunno, 1983: A study of the tornadic region within a supercell thunderstorm. *J. Atmos. Sci.*, **40**, 359–377.
- Koch, S. E., M. DesJardins, and P. J. Kocin, 1983: An interactive Barnes objective map analysis scheme for use with satellite and conventional data. *J. Climate Appl. Meteor.*, **22**, 1487–1503.
- Kosiba, K. and J. Wurman, 2010: The three-dimensional axisymmetric wind field structure of the Spencer, South Dakota (1998) tornado. *In Press, J. Atmos. Sci*
- Lee, W.-C., and J. Wurman, 2005: The diagnosed structure of the Mulhall tornado. *J. Atmos. Sci.*, **62**, 2373–2393.
- Lemon, L. R., and C. A. Doswell, 1979: Severe thunderstorm evolution and mesocyclone structure as related to tornadogenesis. *Mon. Wea. Rev.*, **107**, 1184–1197.

- Ludlam, F. H., 1963: Severe Local Storms: A review. *Severe Local Storms Meteor. Monogr.*, No. 27., 1-30.
- Majcen, M., P. Markowski, Y. Richardson, D. Dowell, and J. Wurman, 2008: Multipass objective analysis of Doppler radar data. *J. Atmos. Oceanic Technol.*, **25**, 1845-1858.
- Markowski, P. M., J. M. Straka, and E. N. Rasmussen, 2002: Direct surface thermodynamic observations within the rear-flank downdrafts of nontornadic and tornadic supercells. *Mon. Wea. Rev.*, **130**, 1692–1721.
- Marquis, J., Y. Richardson, J. Wurman, and P. Markowski, 2008: Single- and dual-Doppler analysis of a tornadic vortex and surrounding storm-scale flow in the Crowell, TX, supercell of 30 April 2000. *Mon. Wea. Rev.*, **136**, 5017-5043.
- Pauley, P. M., and X. Wu, 1990: The theoretical, discrete, and actual response of the Barnes objective analysis scheme for one- and two-dimensional fields. *Mon. Wea. Rev.*, **118**, 1145–1163.
- Potvin, C. K., A. Shapiro, T.-Y. Yu, J. Gao, and M. Xue, 2009: A new multiple-Doppler tornado detection and characterization technique. *Bull. Amer. Meteor. Soc.*, in press.
- Ray, P. S., R. J. Doviak, G. B. Walker, D. Sirmans, J. Carter, and B. Bumgarner, 1975: Dual-Doppler observations of a tornadic storm. *J. Appl. Meteor.*, **14**, 1521-1530.
- , B. C. Johnson, K. W. Johnson, J. S. Bradberry, J. J. Stephens, K. K. Wagner, R. B. Wilhelmson, and J. B. Klemp, 1981: The morphology of severe tornadic storms on 20 May 1977. *J. Atmos. Sci.*, **38**, 1643-1663.
- Richardson, Y., D. Dowell, and J. Wurman, 2001: High resolution dual-Doppler analyses of two thunderstorms during the pretornadogenesis and mature tornado stages. Preprints, *30th Int. Conf. on Radar Meteorology*, Munich, Germany, Amer. Meteor. Soc., 295–297.
- Romine, G. S., L. Wicker, M. Gilmore, L. Counce, and R. B. Wilhelmson, 2004: Analysis of simulated supercell tornadogenesis. *22nd Conference on Severe Local Storms, Hyannis MA, Amer. Meteor. Soc.*
- Rotunno, R., 1984: An investigation of a three-dimensional asymmetric vortex. *J. Atmos. Sci.*, **41**, 283–298.
- , and J. B. Klemp, 1985: On the rotation and propagation of simulated supercell thunderstorms. *J. Atmos. Sci.*, **42**, 271–292.
- Stout, G.E., and F.A. Huff, 1953: Radar records an Illinois tornado. *Bull. Amer. Meteor. Soc.*, **34**, 281-284.

- Tanamachi, R. L., H. B. Bluestein, W.-C. Lee, M. Bell, and A. Pazmany, 2007: Ground based velocity track display (GBVTD) analysis of W-band Doppler radar data in a tornado near Stockton, Kansas, on 15 May 1999. *Mon. Wea. Rev.*, **135**, 783–800.
- Trapp, R. J., 1999: Observations of non-tornadic low-level mesocyclones and attendant tornadogenesis failure during VORTEX. *Mon. Wea. Rev.*, **127**, 1693-1705.
- Wakimoto, R. M., and C. Liu, 1998: The Garden City, Kansas, storm during VORTEX 95. Part II: The wall cloud and tornado. *Mon. Wea. Rev.*, **126**, 393–408.
- , and H. Cai, 2000: Analysis of a nontornadic storm during VORTEX 95. *Mon. Wea. Rev.*, **128**, 565–592.
- Weisman, M. L., and J. B. Klemp, 1984: The structure and classification of numerically simulated convective storms in directionally varying wind shears. *Mon. Wea. Rev.*, **112**, 2479-2498.
- Wicker, L. J., and R. B. Wilhelmson, 1995: Simulation and analysis of tornado development and decay within a three dimensional supercell thunderstorm. *J. Atmos. Sci.*, **52**, 2675–2703.
- Wurman, J., 2002: The multiple-vortex structure of a tornado. *Wea. Forecasting*, **17**, 473–504.
- , and S. Gill, 2000: Finescale radar observations of the Dimmitt, Texas (2 June 1995), tornado. *Mon. Wea. Rev.*, **128**, 2135–2164.
- , and M. Randall, 2001: An inexpensive, mobile, rapid-scan radar. Preprints, 30th *Int. Conf. on Radar Meteorology*, Munich, Germany, Amer. Meteor. Soc., P3.4. [Available online at <http://ams.confex.com/ams/pdfpapers/21577.pdf>.]
- , and C. Alexander, 2004: Scales of motion in tornadoes. What radars cannot see. What scale circulation is a tornado. Preprints, 22nd *Conf. on Severe Local Storms*, Hyannis, MA, Amer. Meteor. Soc., P11.6. [Available online at <http://ams.confex.com/ams/pdfpapers/82353.pdf>.]
- , and ———, 2005: The 30 May 1998 Spencer, South Dakota, storm. Part II: Comparison of observed damage and radar derived winds in the tornadoes. *Mon. Wea. Rev.*, **133**, 97–119.
- , J. Straka, and E. Rasmussen, 1996a: Preliminary radar observations of the structure of tornadoes. Preprints, 18th *Conf. on Severe Local Storms*, San Francisco, CA, Amer. Meteor. Soc., 17–22.
- , ———, and ———, 1996b: Fine scale Doppler radar observations of tornadoes, *Science*, **272**, 1774-1777.

- , ——, ——, M. Randall, and A. Zahrai, 1997: Design and deployment of a portable, pencil-beam, pulsed, 3-cm Doppler radar. *J. Atmos. Oceanic Technol.*, **14**, 1502–1512.
- , Y. Richardson, C. Alexander, S. Weygandt, and P. F. Zhang, 2007a: Dual-Doppler and single-Doppler analysis of a tornadic storm undergoing mergers and repeated tornadogenesis. *Mon. Wea. Rev.*, **135**, 736–758.
- , ——, ——, ——, and ——, 2007b: Dual-Doppler analysis of winds and vorticity budget terms near a tornado. *Mon. Wea. Rev.*, **135**, 2392–2405.
- , P. Robinson, W. –C. Lee, C. R. Alexander, and K. A. Kosiba, 2008: Rapid-scan mobile radar 3D GBVTD and traditional analysis of tornadogenesis. *Proc., 24th Conf. on Severe Local Storms*, Savannah, GA, Amer. Meteor. Soc.

Figure Captions:

Figure 1: The time evolution of the Orleans, Nebraska tornadic supercell, as observed by the Hastings, Nebraska WSR-88D radar (KUEX), during the dual-Doppler analysis period, from 2300 to 2310. The left panels depict reflectivity (dBz) and the right panels depict Doppler velocities (m s^{-1}). Both fields are shown at an elevation of 0.5° . Black circles indicate the approximate locations of DOW2 (D2) and DOW3 (D3). An arrow indicates the location of KUEX (approximately 100 km to the northeast). A supercell thunderstorm with a prominent hook echo and mesocyclone crossed the DOW study area.

Figure 2: The dual-Doppler deployment for the Orleans, Nebraska, supercell. Tornado locations as determined from DOW data, are depicted for several times. The western extent of the dual-Doppler coverage is indicated with the black circle. The tornado crossed north of Orleans and through the dual-Doppler lobe, dissipating just to the west of DOW2.

Figure 3: Single-Doppler radial velocity (m s^{-1} ; left panels) and reflectivity (dBZ; right panels) data collected at several elevation angles by DOW3 at 2254 UTC, before the dual-Doppler observation period commenced. The approximate height of the tornado center in each of scans are indicated on the images. An arrow indicates the direction of DOW3 (D3). The primary rear flank gust front (PRFGF), indicated by a thick black line, is located well to the northeast of the tornado and slopes inward toward the tornado with increasing height. The stippled lines in the subsequent panels indicate the location of the 100 m AGL PRFGF.

Figure 4: Photograph of the Orleans tornado. Time and location not documented.

Figure 5: Single-Doppler radial velocity (m s^{-1}) and reflectivity (dBZ) data collected by DOW2 and DOW3 during the dual-Doppler analysis period. Data are shown at 1° elevation from 2300 To 2309. The black line indicates the position of the PRFGF, the red line indicates the position of the SRFGR, the “X” marks the location of the new circulation north of the tornado, the star marks the location of the DOW3, and the hexagon marks the location of DOW2. During this period the hook echo becomes increasingly enfolded into the main precipitation core of the supercell.

Figure 6: Zoomed in view the tornado (Doppler velocity (m s^{-1}) left, radar reflectivity (dBZ) right) at elevations of 0.4° and 5.0° . The tornado core flow is resolved revealing a core flow diameter of approximately 200 m and a debris ring (at 0.4°).

Figure 7: Time evolution of Doppler velocity difference, spatial scale, estimated vertical vorticity, and estimated circulation from DOW2 and DOW3 single-Doppler data for the Orleans, Nebraska, tornado. Data are taken from the 1.5° elevation scans. At earlier times, from 2255 to 2258, only DOW3 data are available. During this time interval, contraction in scale is associated with increase in vorticity and wind speeds. At later times, from 2259-2307, tornado scale remains relatively constant but wind speeds increase significantly. Finally, after 2307, the tornado wind speeds decrease rapidly while the tornado becomes somewhat narrower.

Figure 8: Convergence (red)/divergence (blue) in s^{-1} and tornado-relative horizontal winds in $m s^{-1}$ of the tornadic region of the storm for two independent dual-Doppler syntheses (2300 and 2307 UTC) at heights of 100 m and 600 m AGL. The black line indicates the location of the PRFGF, the green line indicates the location of the SRFGF, the “T” marks the location of the tornado at both times, and the “X” indicates the location of the secondary circulation north of the tornado at 2307.

Figure 9: Vertical velocities (shaded: red upward, blue downward) and horizontal winds (in $m s^{-1}$) of the tornadic region of the storm for six independent dual-Doppler syntheses at a height of 100 m. The SRFGF is located ahead of the region of downward motion. The black line indicates the location of the PRFGF, the green line indicates the location of the SRFGF, the “T” marks the location of the tornado at both times, and the “X” indicates the location of the secondary circulation north of the tornado at 2307.

Figure 10: Distance from the most intense convergence regions of the PRFGF and SRFGF to the tornado circulation center for volumes 2300, 2301, 2303, 2306, 2307, and 2309. Also shown are the ΔV values for each of these dual-Doppler volumes. Separation of the PRFGF and SRFGF from the tornadic circulation could be related to eventual tornado demise. The dotted line indicates the times when a secondary circulation is present north of the tornado.

Figure 11: Vertical vorticity (shaded) in s^{-1} and horizontal winds in $m s^{-1}$ of the tornadic region of the storm for three independent dual-Doppler syntheses (2301, 2303, and 2307 UTC) at heights of 100 m (left panels) and 600 m (right panels). The maximum vertical vorticity is associated with the tornadic circulation. A secondary vertical vorticity maximum is associated with the PRFGF wrapping around the tornadic region, and becomes associated with the secondary circulation by 2307 UTC. “X” marks the location of the secondary vorticity maximum.

Figure 12: The circulation as a function of radius for eight independent dual-Doppler volumes at a height of 100 m AGL (labeled with UTC time). Circulation increased rapidly with radius immediately away from the tornado, then more slowly farther out. Values changed little with time during intensification or dissipation of the tornado.

Figure 13: Stretching (red)/compression (blue) in s^{-2} and horizontal winds in m s^{-1} of the tornadic region of the storm for three independent dual-Doppler syntheses (2300, 2303, and 2307 UTC) at a height of 100 m AGL. The stretching/compression associated with the tornadic circulation evolves from a stretching/compression dipole at 2300, to an annulus of stretching compression surrounding a region of compression at 2303, to a stretching monopole at 2307. A region of stretching is evident along the PRFGF.

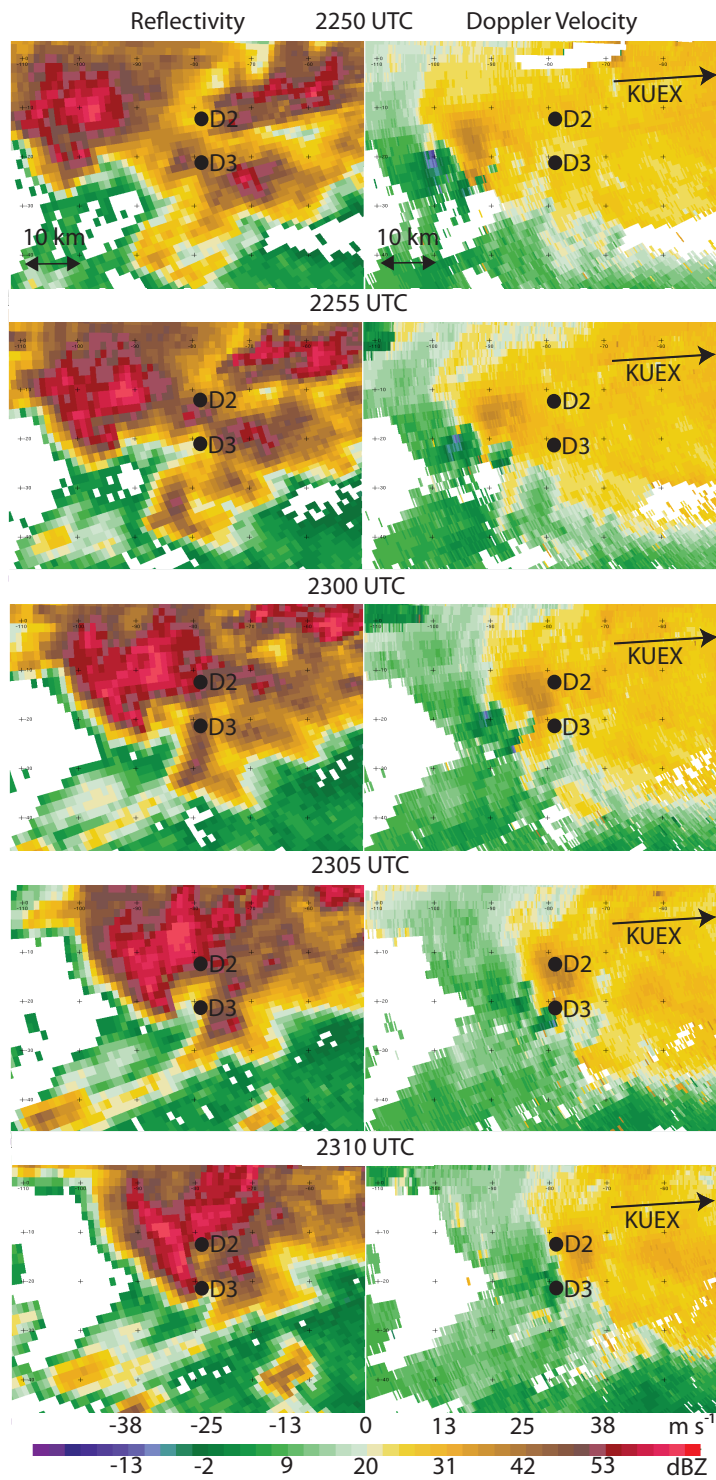


Figure 1: The time evolution of the Orleans, Nebraska tornadic supercell, as observed by the Hastings, Nebraska WSR-88D radar (KUEX), during the dual-Doppler analysis period, from 2300 to 2310. The left panels depict reflectivity (dBZ) and the right panels depict Doppler velocities (m s^{-1}). Both fields are shown at an elevation of 0.5° . Black circles indicate the approximate locations of DOW2 (D2) and DOW3 (D3). An arrow indicates the direction of KUEX (approximately 100 km to the northeast). A supercell thunderstorm with a prominent hook echo and mesocyclone crossed the DOW study area.

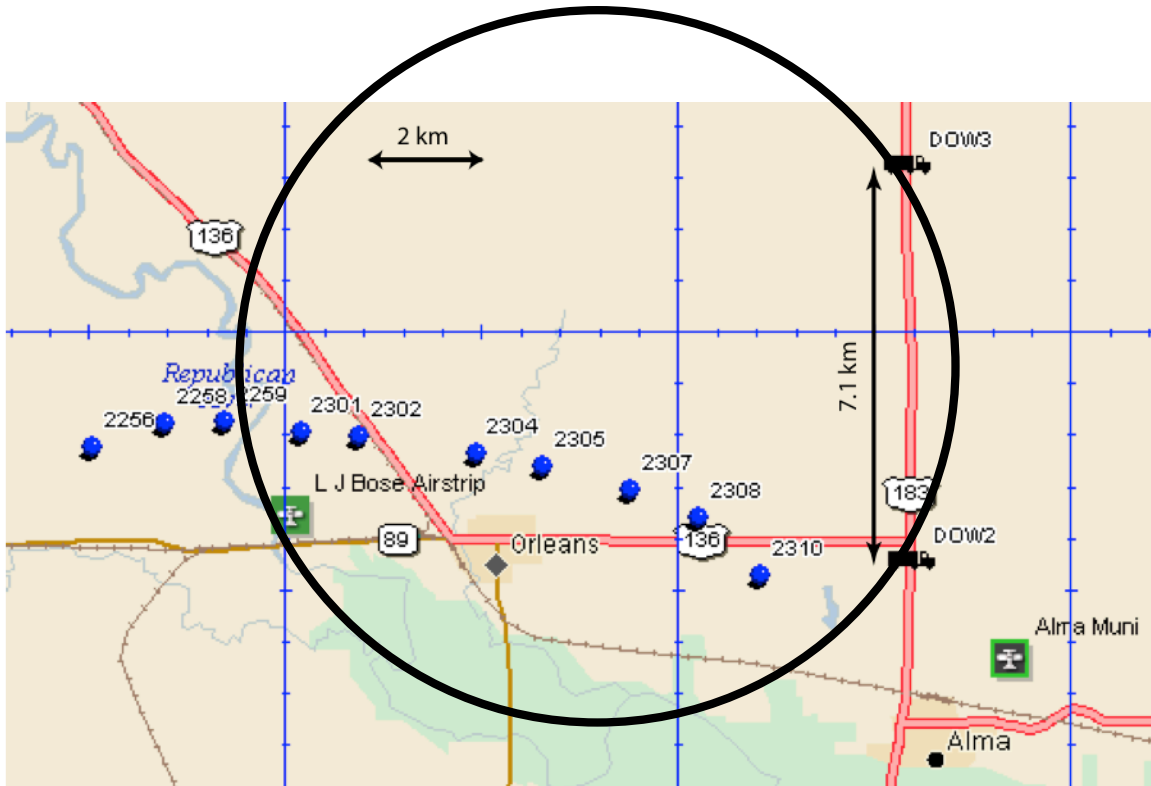


Figure 2: The dual-Doppler deployment for the Orleans, Nebraska, supercell. Tornado locations, as determined from DOW data, are depicted for several times. The western extent of the dual-Doppler coverage is indicated with the black circle. The tornado crossed north of Orleans and through the dual-Doppler lobe, dissipating just to the west of DOW2.

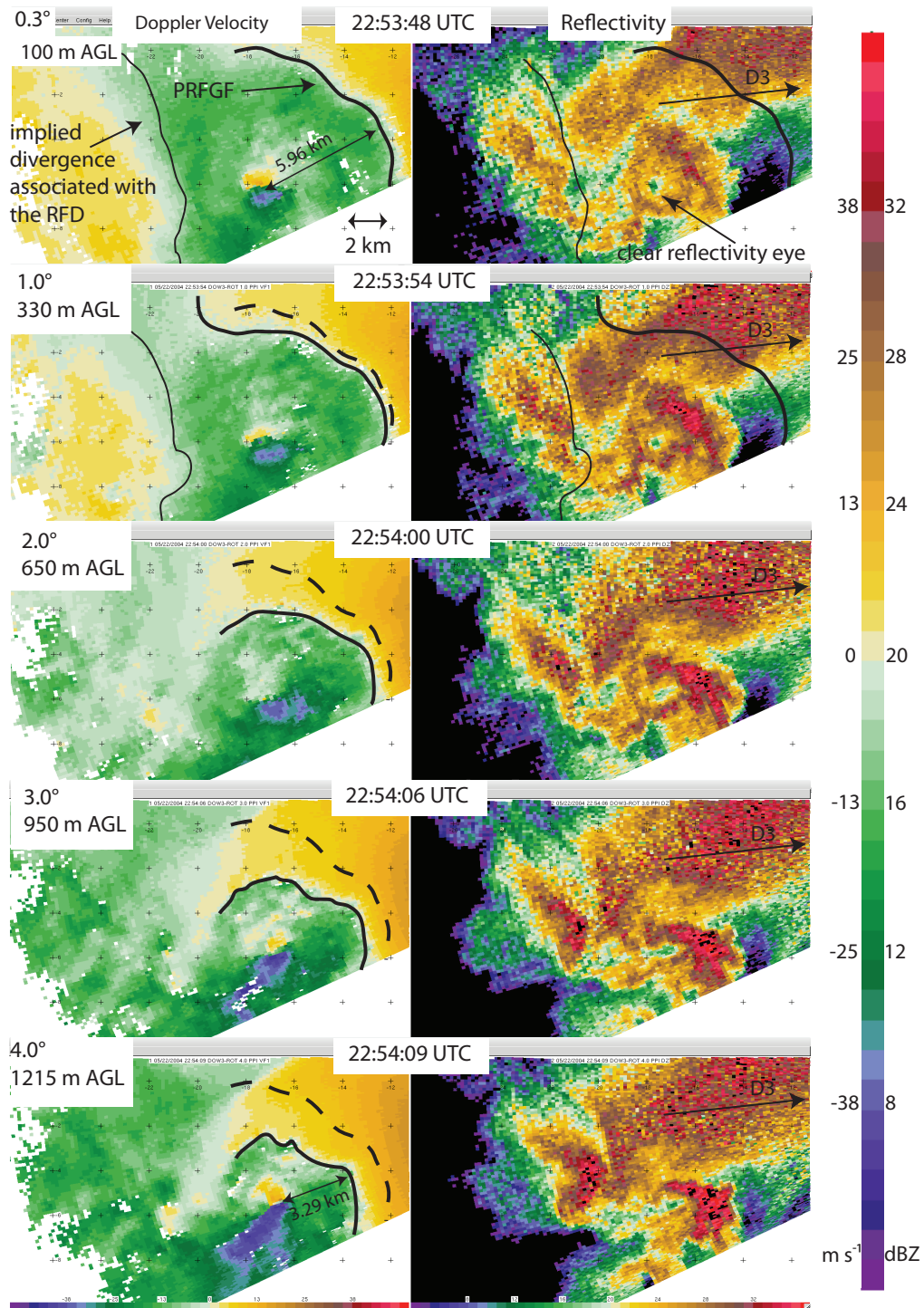


Figure 3: Single-Doppler radial velocity (m s^{-1} ; left panels) and reflectivity data (dBZ; right panels) collected at five elevation angles by DOW3 at 2254 UTC, before the dual-Doppler observation period commenced. The approximate time and height of the tornado center of each scan are indicated on the images. An arrow indicates the direction of DOW3 (D3). The primary rear flank gust front (PRFGF), indicated by a thick black line, is located well to the northeast of the tornado and slopes inward toward the tornado with increasing height. The stippled lines in the subsequent panels indicate the location of 100 m AGL PRFGF.



Figure 4. Photograph of the Orleans tornado. Time not documented.

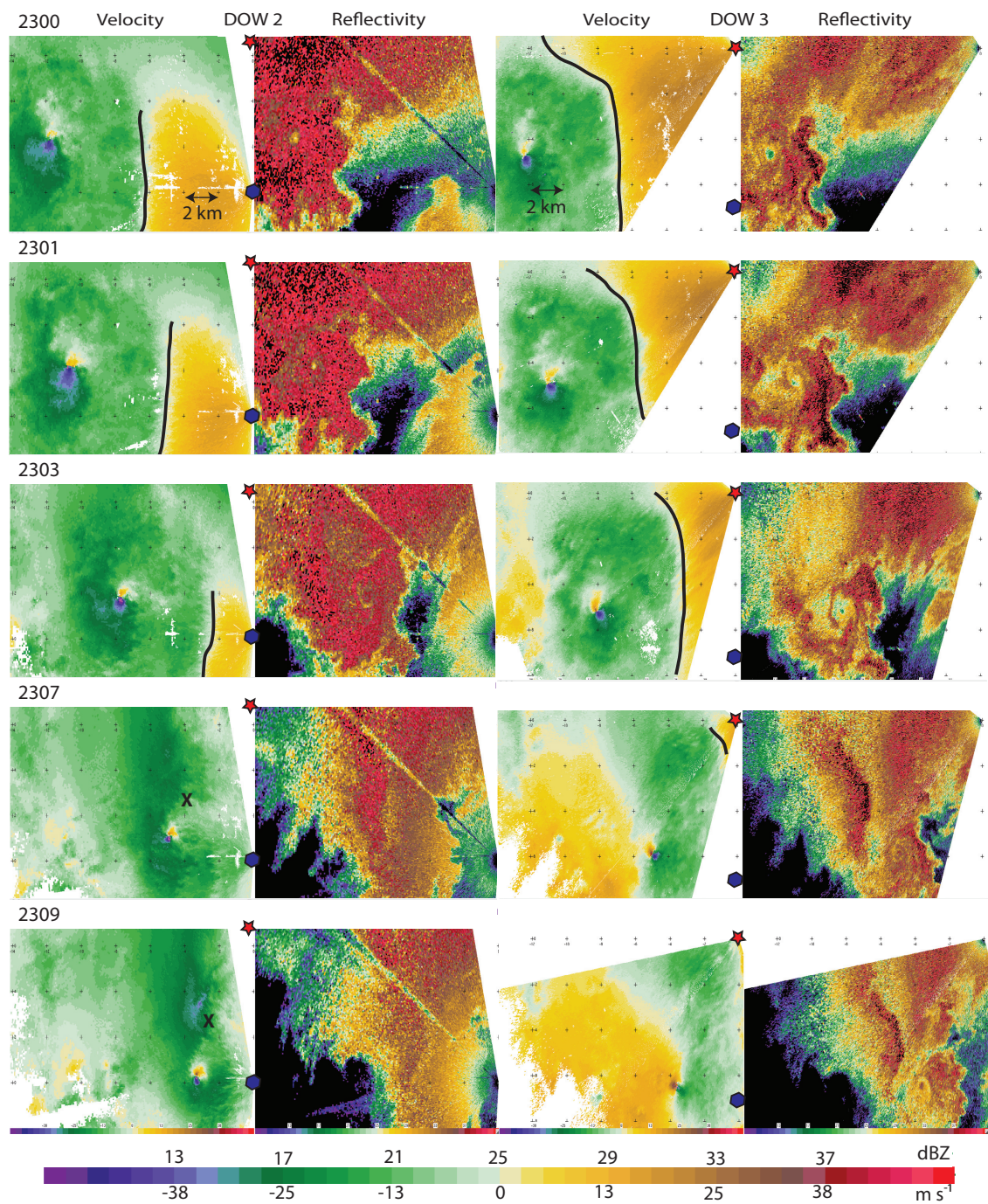


Figure 5. Single-Doppler radial velocity (m s^{-1}) and reflectivity (dBZ) data collected by DOW2 and DOW3 during the dual-Doppler analysis period. Data are shown at 1° elevation from 2300 to 2309. The black line indicates the position of the PRFGF, the "X" marks the location of the new circulation north of the tornado, the star marks the location of the DOW3, and the hexagon marks the location of DOW2. During this period the hook echo becomes increasingly enfolded into the main precipitation core of the supercell.

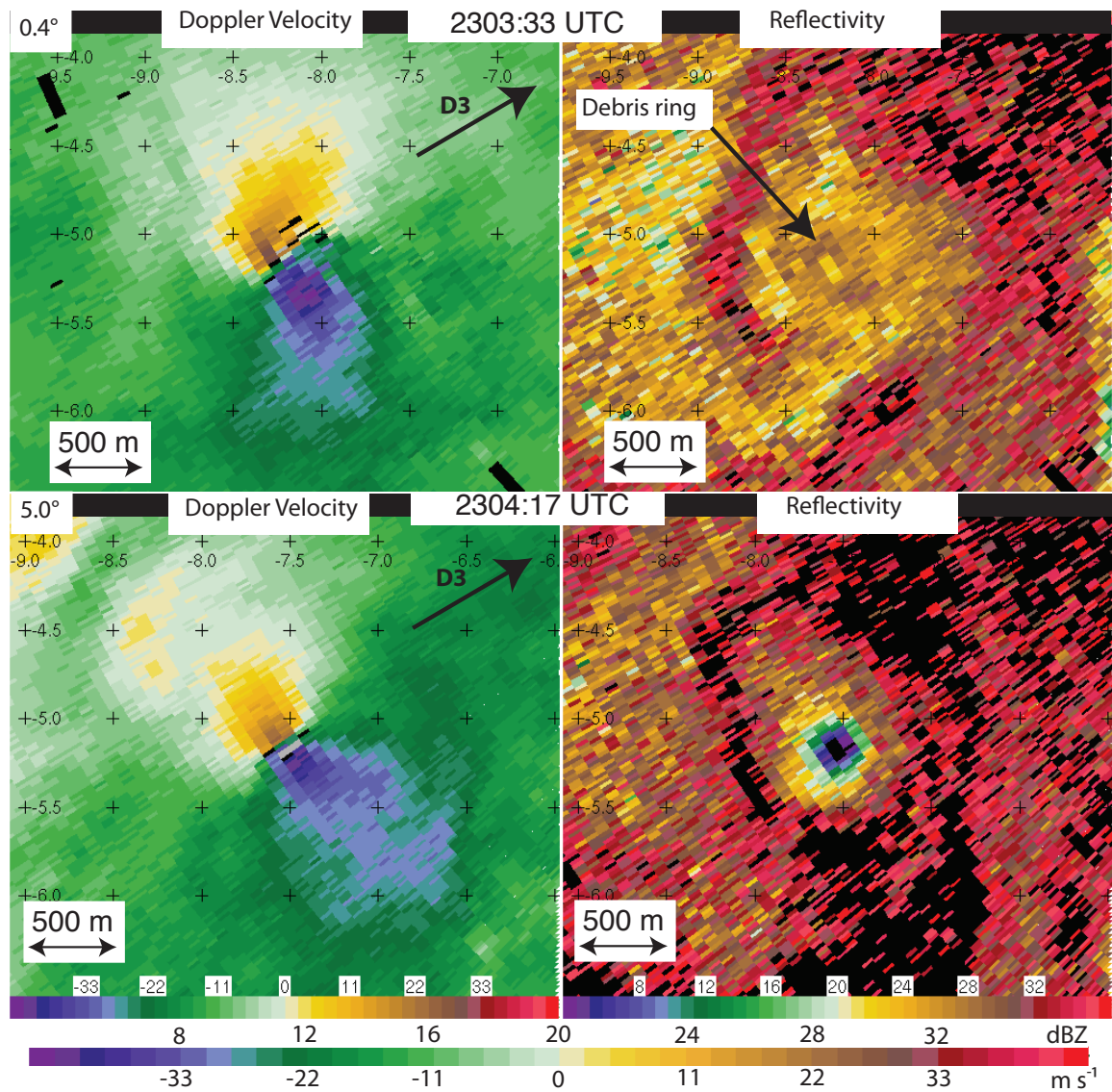


Figure 6. Zoomed in view the tornado (Doppler velocity (m s^{-1}) left, radar reflectivity (dBZ) right) at elevations of 0.4° and 5.0°. The tornado core flow is resolved revealing a core flow diameter of approximately 200 m and a debris ring (at 0.4°).

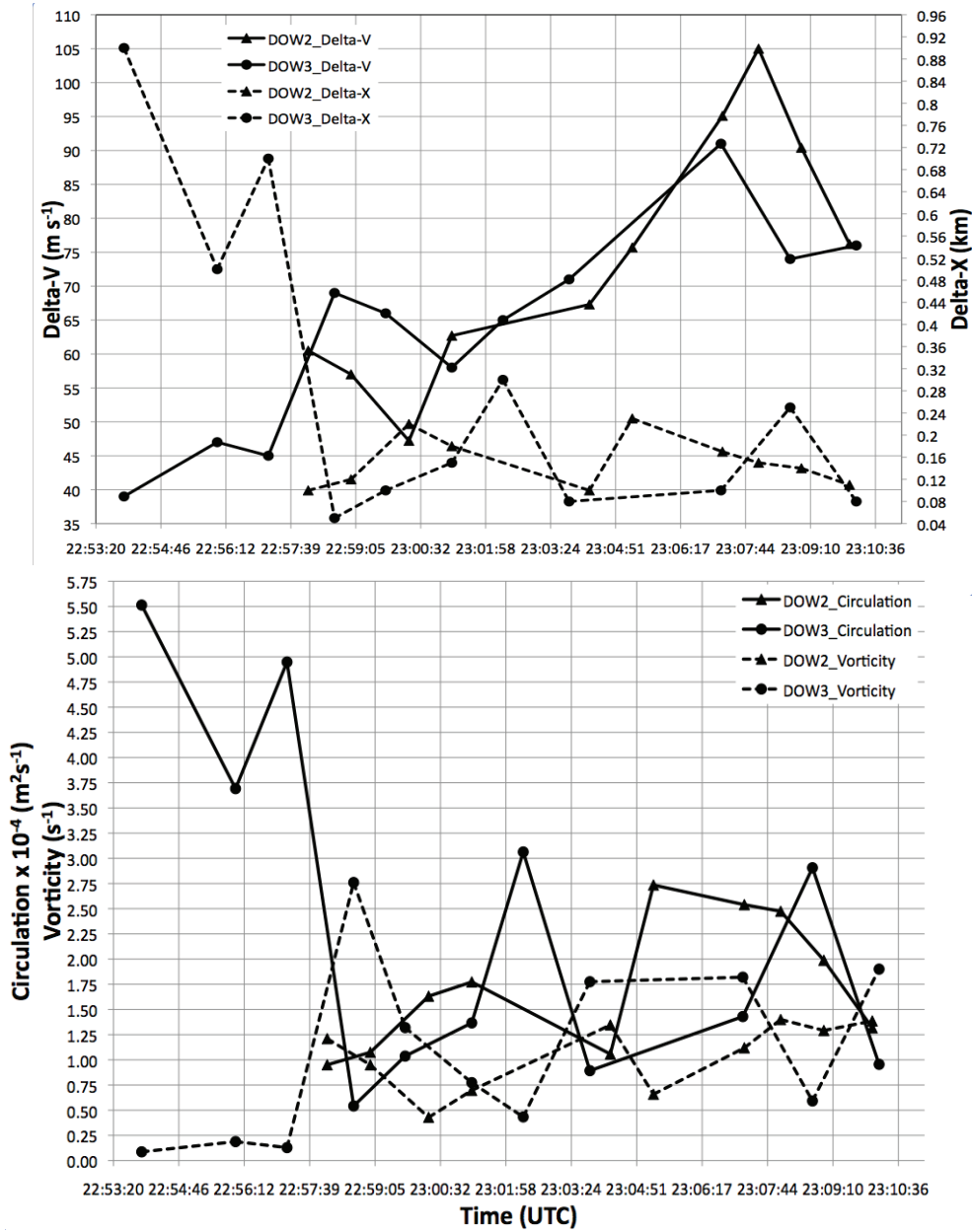


Figure 7. Time evolution of Doppler velocity difference, spatial scale, estimated vertical vorticity, and estimated circulation from DOW3 single-Doppler data for the Orleans, Nebraska, tornado. Contraction in scale is associated with increase in vorticity and wind speeds at early times, from 2255-2258. At later times, from 2259-2307, tornado scale remains relatively constant but wind speeds increase significantly. Finally, after 2307, the tornado wind speeds decrease rapidly while the tornado becomes somewhat narrower.

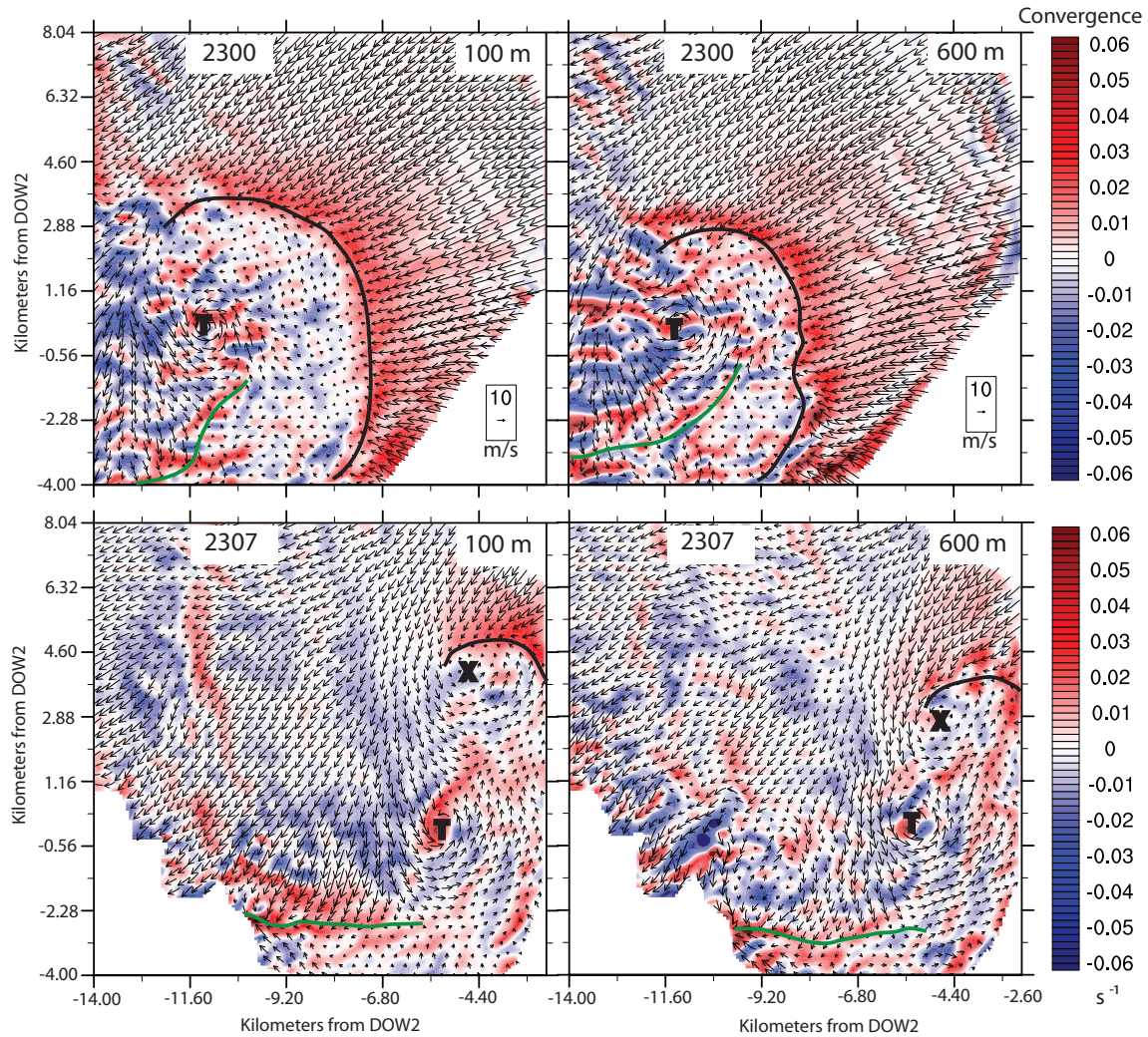


Figure 8. Convergence (red)/divergence (blue) in s^{-1} and tornado-relative horizontal winds in $m s^{-1}$ of the tornadic region of the storm for two independent dual-Doppler syntheses (2300 and 2307 UTC) at heights of 100 m and 600 m AGL. The black line indicates the location of the PRFGF, the green line indicates the location of the SRFGF, the “T” marks the location of the tornado at both times, and the “X” indicates the location of the secondary circulation north of the tornado at 2307.

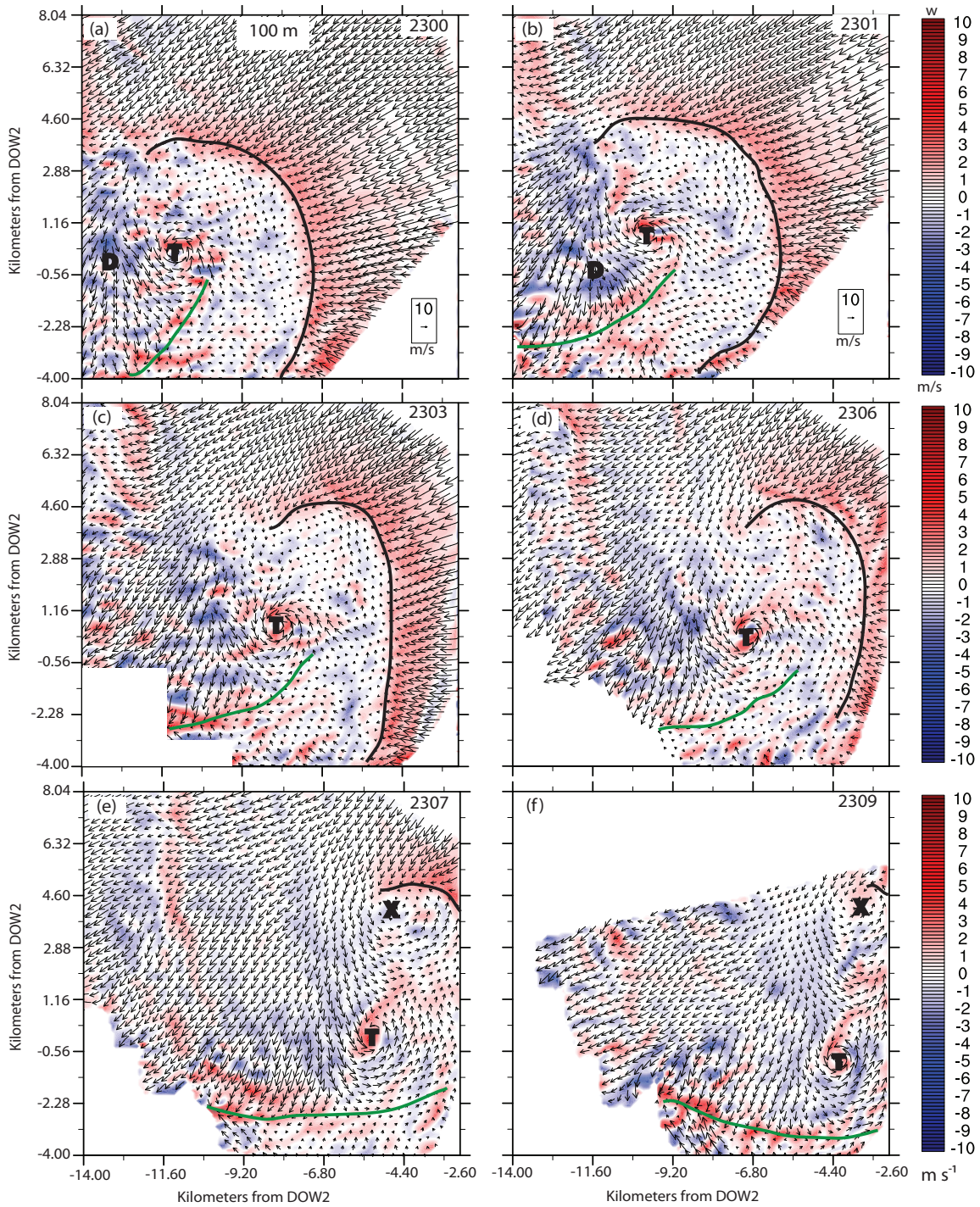


Figure 9. Vertical velocities (shaded: red upward, blue downward) and horizontal winds (in m s^{-1}) of the tornadic region of the storm for six independent dual-Doppler syntheses at a height of 100 m. The SRFGF is located ahead of the region of downward motion. The black line indicates the location of the PRFGF, the green line indicates the location of the SRFGF, the “T” marks the location of the tornado at both times, and the “X” indicates the location of the secondary circulation north of the tornado at 2307.

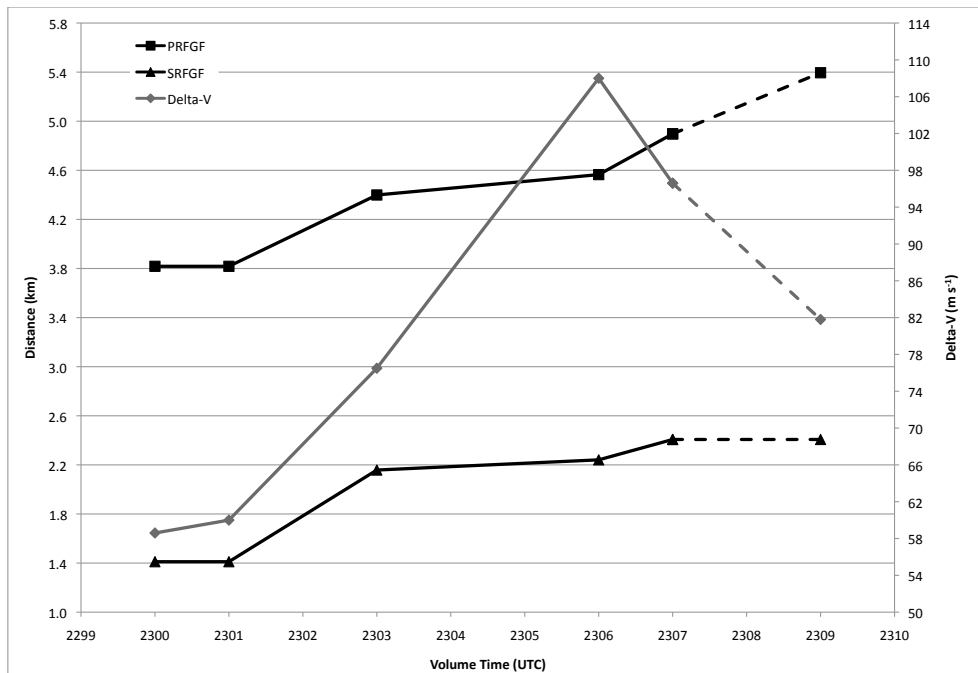


Figure 10. Distance from the most intense convergence regions of the PRFGF and the SRFGF to the tornado circulation center for volumes 2300, 2301, 2303, 2306, 2307, and 2309. Also shown are the ΔV values for each of these dual-Doppler volumes. Separation of the PRFGF and SRFGF from the tornadic circulation could be related to eventual tornado demise. The dotted line indicates the times when a secondary circulation is present north of the tornado.

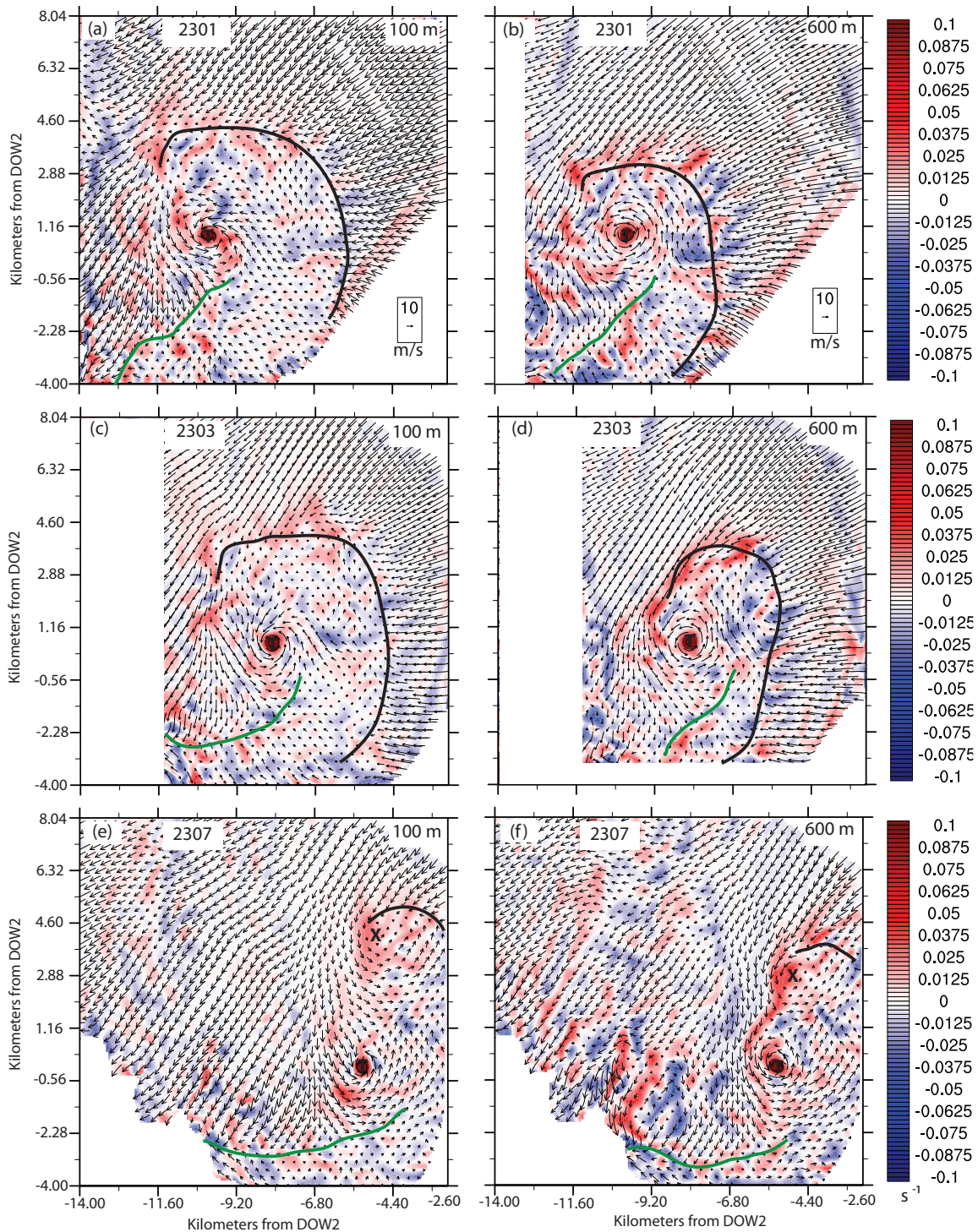


Figure 11. Vertical vorticity (shaded) in s^{-1} and horizontal winds in $m s^{-1}$ of the tornadic region of the storm for three independent dual-Doppler syntheses (2301, 2303, and 2307 UTC) at heights of 100 m (left panels) and 600 m (right panels). The maximum vertical vorticity is associated with the tornadic circulation. A secondary vertical vorticity maximum is associated with the PRFGF wrapping around the tornadic region, and becomes associated with the secondary circulation by 2307 UTC.

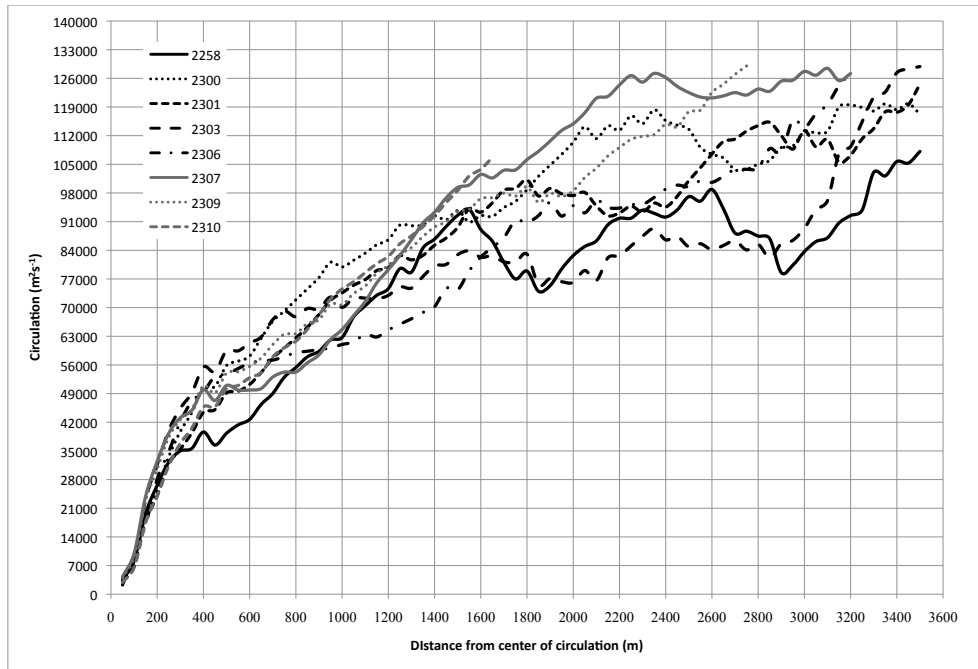


Figure 12. The circulation as a function of radius for eight independent dual-Doppler volumes at a height of 100 m AGL (labeled with UTC time). Circulation increased rapidly with radius immediately away from the tornado, then more slowly farther out. Values changed little with time during intensification or dissipation of the tornado.

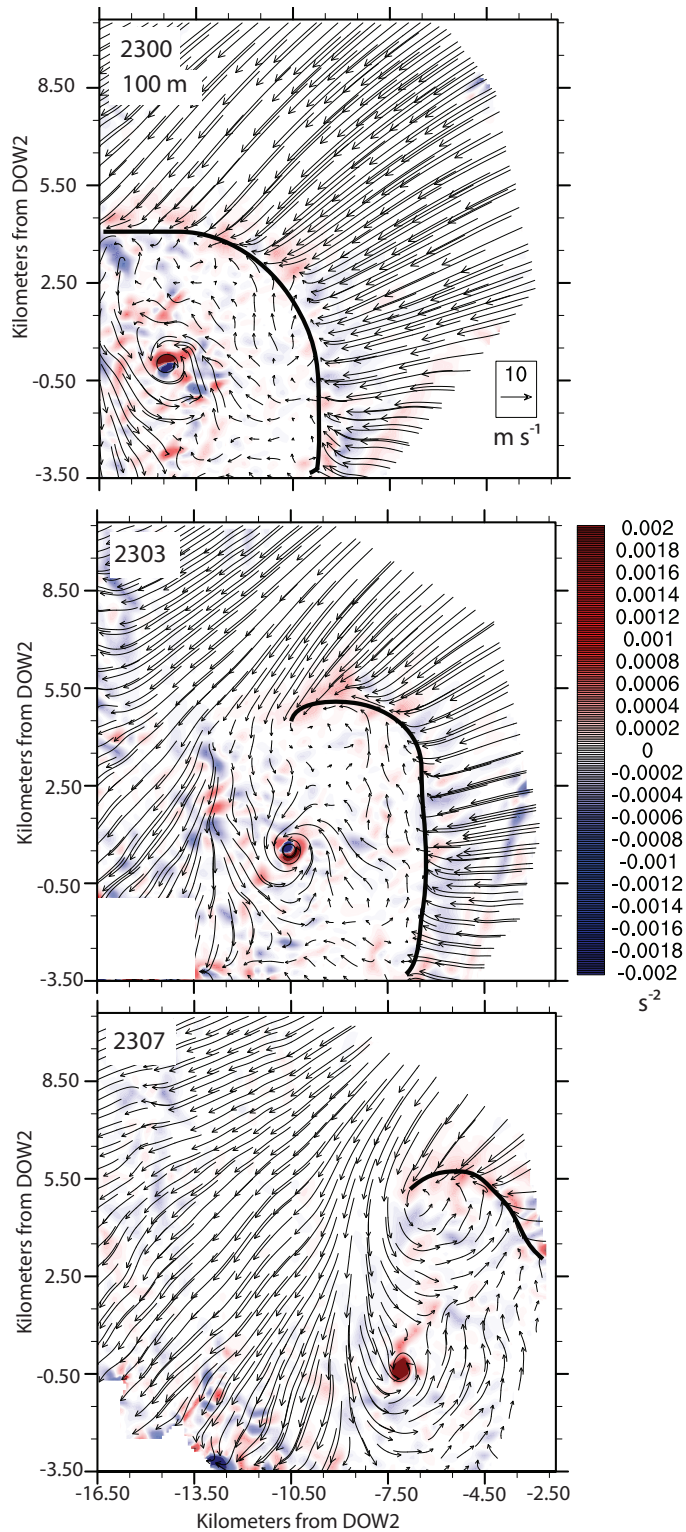


Figure 13. Stretching (red)/compression (blue) in s^{-2} and horizontal winds in $m s^{-1}$ of the tornadic region of the storm for three independent dual-Doppler syntheses (2300, 2303, and 2307 UTC) at a height of 100 m AGL. The stretching/compression associated with the tornadic circulation evolves from a stretching/compression dipole at 2300, to an annulus of stretching compression surrounding a region of compression at 2303, to a stretching monopole at 2307. A region of stretching is evident along the PRFGF.